Journal of Medicinal Chemistry

Article

pubs.acs.org/jmc

Prospective Evaluation of Free Energy Calculations for the Prioritization of Cathepsin L Inhibitors

Bernd Kuhn,[†,#] Michal Tichý,[‡,#] Lingle Wang,[§,#] Shaughnessy Robinson,[§] Rainer E. Martin,[†] Andreas Kuglstatter,[†] Jörg Benz,[†] Maude Giroud,[‡] Tanja Schirmeister,[∥] Robert Abel,[*,§] François Diederich,[*,‡] and Jérôme Hert[*,†]

[†]Roche Pharmaceutical Research and Early Development (pRED), Roche Innovation Center Basel, F. Hoffmann-La Roche Ltd., Grenzacherstrasse 124, 4070 Basel, Switzerland

[‡]Laboratorium für Organische Chemie, ETH Zurich, Vladimir-Prelog-Weg 3, 8093 Zurich, Switzerland

[§]Schrödinger, Inc., 120 West 45th Street, New York, New York 10036, United States

[∥]Institut für Pharmazie und Biochemie, Johannes Gutenberg-Universität Mainz, Staudinger Weg 5, 55128 Mainz, Germany

Supporting Information

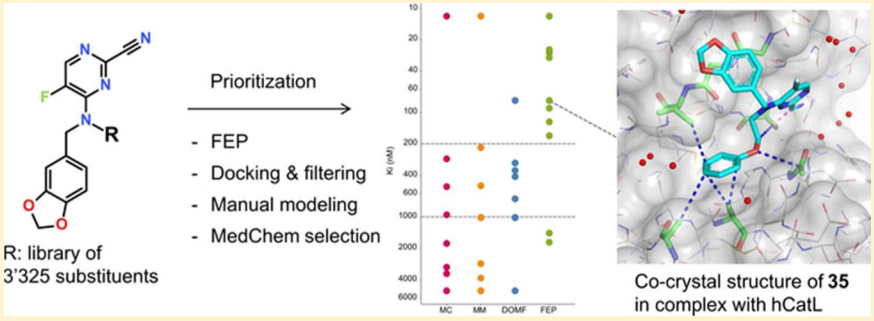

ABSTRACT: Improving the binding affinity of a chemical series by systematically probing one of its exit vectors is a medicinal chemistry activity that can benefit from molecular modeling input. Herein, we compare the effectiveness of four approaches in prioritizing building blocks with better potency: selection by a medicinal chemist, manual modeling, docking followed by manual filtering, and free energy calculations (FEP). Our study focused on identifying novel substituents for the apolar S2 pocket of cathepsin L and was conducted entirely in a prospective manner with synthesis and activity determination of 36 novel compounds. We found that FEP selected compounds with improved affinity for 8 out of 10 picks compared to 1 out of 10 for the other approaches. From this result and other additional analyses, we conclude that FEP can be a useful approach to guide this type of medicinal chemistry optimization once it has been validated for the system under consideration.

INTRODUCTION

Free energy calculation approaches, such as free energy perturbation (FEP), have been around for a long time[1−5] but had only limited impact in the drug discovery process so far. Likely reasons for their historically restrained use include lengthy simulation times not practical in fast-paced project environments combined with overstated accuracy levels based on small test set retrospective analyses which did not translate when employed prospectively in real-world systems. FEP has now taken advantage of improved sampling algorithms[6,7] and force-field quality[8] and is profiting from the increased availability of low-cost parallel computing. Speed and accuracy appear to have progressed significantly.[7,9,10] This has in turn led to recent accounts of successful industrial applications of FEP in active drug discovery projects.[11−13]

Here, we investigate the application of FEP in a typical drug discovery use case where the goal is to prioritize compounds for synthesis. One way for therapeutic project teams to further explore the structure−activity relationship (SAR) of a hit series is to engage in parallel synthesis: A common setting involves a scaffold with one or several defined exit vectors and a set of chemical reactions with the goal of optimizing side chains. The number of suitable reactants accessible (internally or purchasable) can be very large (hundreds, thousands, or more). The task of molecular modeling consists then in prioritizing building blocks with respect to binding affinity in order to limit the amount of synthesis and experimental testing required.

A prerequisite for this exercise is the availability of an initial ligand together with structural information, an experimental cocrystal structure describing the binding mode to the protein. We picked human cathepsin L (hCatL), a cysteine protease, which can be inhibited by ligands with an activated nitrile group forming a covalent thioimidate adduct with the catalytic Cys25. Previous SAR and structural studies with aryl nitriles (Figure 1)

Received: December 28, 2016

ACS Publications © XXXX American Chemical Society

DOI: 10.1021/acs.jmedchem.6b01881
J. Med. Chem. XXXX, XXX, XXX−XXX

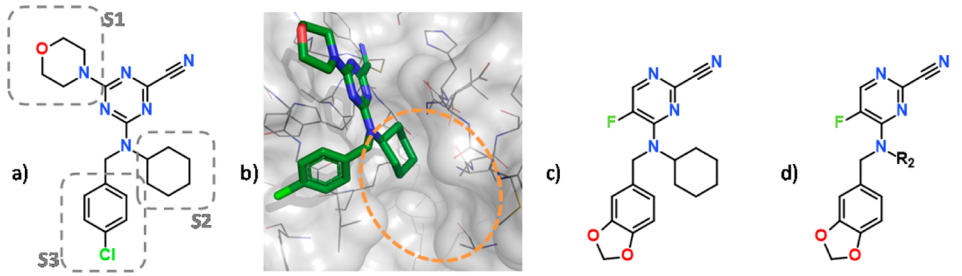

Figure 1. (a) Triazine nitrile reference compound **1**.[16] The substituents in the S1, S2, and S3 pockets of cathepsin L are highlighted with gray dashed-line boxes. (b) Binding mode of compound **1** in hCatl (PDB code 4AXM). The dashed orange circle highlights the region of the S2 pocket. (c) Fluoropyrimidine nitrile reference compound **2**.[15] (d) Fluoropyrimidine nitrile scaffold used in this study.

revealed that apart from the covalent bond the main protein−ligand interactions are made in the S2 and S3 pockets.[14−16] While the reactivity of the aryl nitrile warhead and substituents for the S3 pocket have been explored already to a larger extent, SAR knowledge in the S2 pocket is very limited for this scaffold. As one of the exit vectors at the central nitrogen atom is pointing into the S2 pocket (Figure 1) and is amenable to diverse chemical modifications, we chose this as model system for our investigation.

We evaluated the current state-of-the-art of FEP in prioritizing novel substituents with improved target binding for the S2 pocket of hCatL. The approach was first validated using the S2 pocket SAR available from the literature. The evaluation was then conducted by setting up a realistic drug discovery scenario: Prioritization was carried out in a prospective manner, and FEP predictions were delivered in a constraint time frame that matches project requirements. The performance of FEP is compared to that of established computational approaches as well as to the selection of a medicinal chemist which is used as a benchmark to the theoretical methods. Given the nature of the hCatL system, we believe this study also represents the first account of FEP calculations applied to covalent inhibitors.

RESULTS AND DISCUSSION

Drug Target, Reference Scaffold, and Building Block Selection. The goal of this study is to compare different approaches in their ability to select 10 reactants from a sizable list of available building blocks for array chemistry, which when incorporated into the ligand will yield tight binding with the target protein. Due to the availability of a relevant protein−ligand crystal structure, a reliable biochemical assay for measuring binding affinities, and established chemical synthesis, we chose the drug target hCatL in complex with an aryl nitrile scaffold as model system (Figure 1). Only few substituents have been reported for the S2 pocket, most of them on the triazine nitrile series.[16] The reference compound **1** has an inhibition constant of 13 nM against hCatL, and the binding mode is known from its cocrystal structure (Figure 1a,b). Since this compound already exhibits a high affinity for the target, we decided to base our exploration of the S2 pocket on reference compound **2** (see Figure 1c) which has a reduced reactivity of the warhead resulting in a lower hCatL affinity (K_i = 200 nM).[15] The scaffold resulting from compound **2** used in this experiment is shown in Figure 1d.

The S2 substituent is incorporated in the first of a three-step synthetic route, calling for primary amines for the reductive amination of piperonal (see Experimental Section). We compiled a list of 3325 amines that would lead to fluoropyrimidine compounds with molecular weight of ≤500 Da and that were available in sufficient quantity to carry out the synthesis. The challenge consisted for each submitter to pick 10 building blocks that would result in fluoropyrimidine nitrile derivatives with improved hCatL potency compared to compound **2**.

Each participant had access to the full list of 3325 amines, the list of corresponding fluoropyrimidine compounds (see Supporting Information Table S1), all available SAR on the series (see Supporting Information Table S2), and 1 month of time.[14−16] Building blocks were selected by one of the following four approaches (full details are available from the Experimental Section):

(1) A medicinal chemist without knowledge of hCatL biostructure information browsed through the list of available building block taking previously known SAR into account; this corresponds to our null hypothesis, since no modeling approach was employed (hereafter referred to as MC).
(2) Experts visually assessed the binding mode of compounds minimized with Moloc[17] (MAB force field) and manually selected building blocks based on assumed favorable interactions (hereafter MM).
(3) An expert visually assessed the binding mode of compounds docked with Gold, refined using the MAB force field,[17] rescored with ScorpionScore,[18] and further filtered for highly strained conformations and unfavorable interactions (hereafter DOMF).
(4) As a prerequisite, the FEP approach was validated using the S2 pocket SAR previously published in the literature (see Supporting Information S3). The selection was based on FEP binding free energy estimations for a set of 93 ligands which remained after processing the full reactant set with Glide SP docking, MM-GB/SA scoring, and by-eye diversity analysis (hereafter FEP).

The four sets of selected building blocks are listed in Table 1. Three building blocks (**3**, **13**, **20**) were selected by more than one approach.

Ligand Binding Affinities, Physical Properties, and Comparison of Selection Approaches. All corresponding fluoropyrimidine nitriles were then synthesized except compound **12** for which the synthesis was not successful (see

DOI: 10.1021/acs.jmedchem.6b01881
J. Med. Chem. XXXX, XXX, XXX−XXX

Table 1. List of the Building Blocks Selected by Each of the Four Approaches[e]

Medicinal Chemist (MC)	Manual Modeling (MM)	Docking + Manual filtering (DOMF)	Docking + FEP+ (FEP)
3 	13 	22 	30 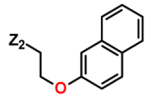
4 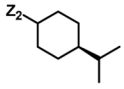	3 	13 	31 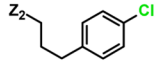
5 	14 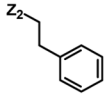	23 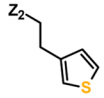	3 
6 	15 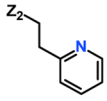	24 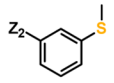	32 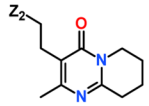
7 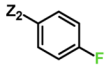	16 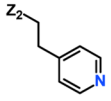	25[b] 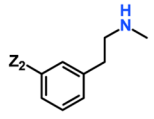	33 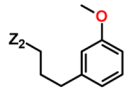
8 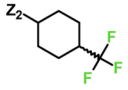	17 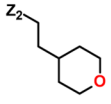	20 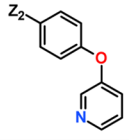	34 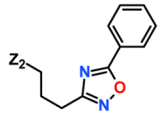
9 	18 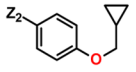	26 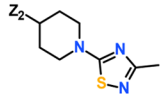	35 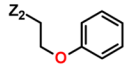
10 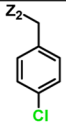	19 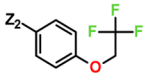	27 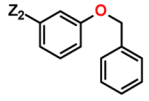	36 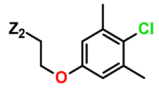
11 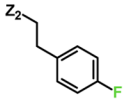	20 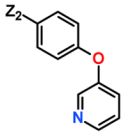	28 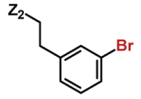	37 
12[a] 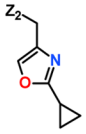	21 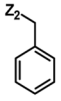	29[c] 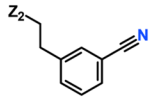	38[d] 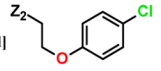

[a]Compound **12** could not be synthesized. [b]Compound **25** is missing a methyl on the nitrogen compared to the intended molecule, still maintaining the positive charge. [c]Compound **29** is an unintended product but was approved in the DOMF approach before compounds were tested. It shows high similarity to compound **28**. [d]The original submission for compound **38** had one more carbon atom in the linker. [e]Three building blocks (**3**, **13**, **20**) were prioritized by more than one approach.

Experimental Section for full details), and their inhibitory constants (K_i) were determined experimentally in a fluorescence-based assay.[14,19] Table 2 provides all details of calculated and measured properties as well as hCatL K_i values, ligand efficiencies[20] (LE), lipophilic efficiencies[21] (LipE) and similarities to the nearest neighbor (see details in the Methods Section) in the set of known fluoropyrimidine nitriles. Of the 36 compounds synthesized and tested, 9 achieved better potency than the reference compound **2**. Compound **3** was picked by three approaches (MC, MM, and FEP), compound **22** was selected by the DOMF approach, and all other compounds were selected by FEP.

Figure 2 shows scatter plots of the inhibitory constants, ligand efficiencies, and lipophilic efficiencies grouped by selection method. The FEP approach was able to pick building blocks that corresponded to compounds with affinities of <200 nM for 8 out of its 10 choices. The other approaches, MC, MM, and DOMF, were each only successful in one case. Looking at a less stringent criterion, the ability to prioritize active compounds (compounds with submicromolar activity, $K_i \leq 1000$ nM, are classified as active, and **13** and **20** with K_i

DOI: 10.1021/acs.jmedchem.6b01881
J. Med. Chem. XXXX, XXX, XXX−XXX

Table 2. Calculated (Molecular Weight, AlogP) and Measured (log *D* and Kinetic Solubility) Properties, hCatL Inhibitory Constant, Corresponding Ligand and Lipophilic Efficiencies (LE and LipE, Respectively), and Nearest Neighbor Tanimoto Similarity (NNT) for the Set of Fluoropyrimidines 3−38

compd	selected by	molecular weight	AlogP	log *D*	kin. sol.	hCatL K_i (nM)[a]	LE	LipE	NNT
3	MC, MM, FEP	354.4	4.0		<0.2	12	0.42	3.90	0.733
4	MC	396.5	5.1	2.74	<0.2	3020	0.26	0.41	0.860
5	MC	326.3	3.0	3.38	0.3	>5100	<0.24	<1.31	0.672
6	MC	348.3	3.9	3.44	<0.2	1800	0.30	1.86	1.000
7	MC	366.3	4.1	3.49	<0.2	952	0.30	1.93	0.852
8 (cis)	MC	422.4	4.8		<0.2	3500	0.25	0.70	0.875
8 (trans)	MC	422.4	4.8		<0.2	>5100	<0.20	<−0.46	0.875
9	MC	372.4	2.9	3.61	0.4	515	0.33	3.41	0.873
10	MC	396.8	4.5		<0.2	>5100	<0.21	<−0.25	0.741
11	MC	394.4	4.4		<0.2	279	0.31	2.15	0.717
13	MM, DOMF	340.4	3.8		<0.2	1010	0.33	2.24	0.721
14	MM	376.4	4.2		<0.2	217	0.33	2.47	0.717
15	MM	377.4	3.2	3.39	4.2	3860	0.26	2.23	0.692
16	MM	377.4	3.0	3.15	<0.2	505	0.31	3.25	0.694
17	MM	384.4	3.1	3.46	<0.2	2790	0.27	2.46	0.662
18	MM	418.4	4.7		<0.2	>5100	<0.19	<−0.39	0.719
19	MM	446.4	4.9		<0.2	>5100	<0.18	<−0.58	0.730
20	MM, DOMF	441.4	4.3		<0.2	1020	0.25	1.70	0.723
21	MM	362.4	3.9		<0.2	>5100	<0.22	<0.42	0.768
22	DOMF	326.3	3.1	3.02	<0.2	77	0.40	4.00	0.729
23	DOMF	382.4	3.9		<0.2	671	0.31	2.32	0.662
24	DOMF	394.4	4.4		<0.2	5100	0.26	0.87	0.770
25	DOMF	405.4	3.7		<0.2	>5100	<0.195	<0.55	0.734
26	DOMF	453.5	2.9	3.49	0.4	411	0.27	3.49	0.716
27	DOMF	454.5	5.5		<0.2	>5100	<0.17	<−1.16	0.778
28	DOMF	455.3	4.9		<0.2	358	0.30	1.50	0.652
29	DOMF	401.4	4.1	2.12	<0.2	304	0.30	2.44	0.662
30	FEP	442.4	4.8		<0.2	123	0.29	2.08	0.614
31	FEP	424.9	5.3		<0.2	27	0.34	2.25	0.672
32	FEP	462.5	3.0	2.96	18	1750	0.23	2.75	0.557
33	FEP	420.4	4.6		<0.2	30	0.33	2.89	0.629
34	FEP	458.4	4.0			91	0.28	3.01	0.597
35	FEP	392.4	3.9		<0.2	77	0.34	3.19	0.672
36	FEP	454.9	5.6	2.32	<0.2	1430	0.25	0.29	0.638
37	FEP	368.3	3.0	3.16	0.5	25	0.40	4.59	0.717
38	FEP	426.8	4.6		<0.2	167	0.31	2.19	0.642

[a]Result is the average of three independent measurements.

values of 1010 nM and 1020 nM, respectively, are included), MC has a success rate of 40%, MM of 50%, DOMF of 70%, and FEP of 80%. In total, there were only three compounds **3**, **22**, and **37** that had better ligand efficiencies than reference compound **2** with FEP identifying two of those. This is perhaps surprising as the ligand efficiency of **2** was not that high to begin with (0.35), even though improving ligand efficiency was not one of the initially stated objectives. Lipophilic efficiency was better than compound **2** for 10 of the new fluoropyrimidines. MC, MM, and DOMF each identified two of those, and FEP identified six of them.

From these results, it is clear that FEP outperformed all other approaches in prioritizing compounds for this particular system. The scatterplots in Figure 2 show that this is most pronounced when inhibitory constants are compared. For LE and LipE, the difference from the other methods is smaller, reflecting the fact that submissions using FEP generally involved larger and more lipophilic substituents. The S2 pocket is quite hydrophobic, and it is possible that the trend of identifying more lipophilic R-groups may simply be a function of the specifics of that pocket rather than a feature of the optimization method. Additional studies in more polar binding sites are required to address this point.

All fluoropyrimidine compounds obtained from the complete set of 3325 building blocks have an average similarity to previously reported inhibitors of 0.643 (see Experimental Section for details on the similarity calculation). The average similarity of the molecules of the MC submission is significantly higher, 0.820, suggesting that the selected molecules are closely related to the known inhibitors and more so than could be expected from a representative selection. The average similarity of the MM and DOMF molecules is also higher than that of the whole set with 0.716 and 0.715, respectively. In contrast, the average similarity of molecules selected by FEP is 0.647, in line with the average of the whole pool of candidates.

The nine newly synthesized hCatL inhibitors with improved binding have topologies that fall into two classes, hereafter termed A and B. Molecules of class A contain a small lipophilic motif adjacent to a methylene linker (**3**, **22**, **37**). This topology was previously unknown and unreported though ligands **3**, **22**,

DOI: 10.1021/acs.jmedchem.6b01881
J. Med. Chem. XXXX, XXX, XXX−XXX

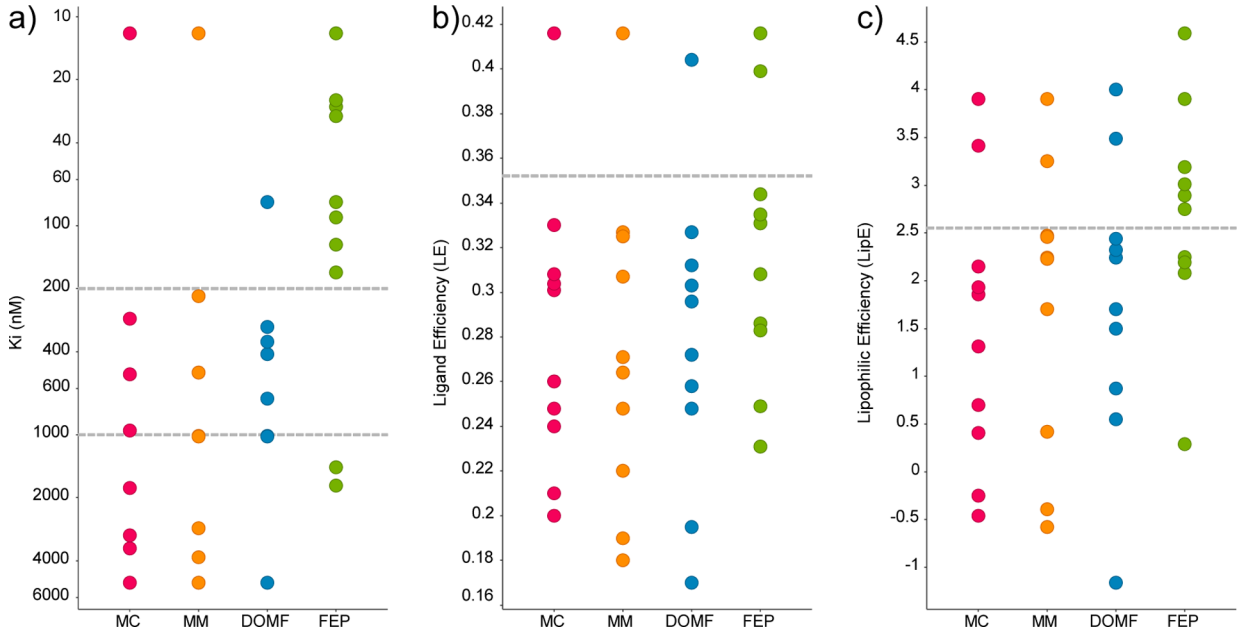

Figure 2. Scatter plots displaying (a) the inhibitory constant K_i, (b) ligand efficiency,[20] and (c) lipophilic efficiency[21] of the fluoropyrimidine nitrile compounds **3**–**38** grouped by selection method (MC = pink, MM = orange, DOMF = blue, and FEP = green). The dashed lines indicate the K_i, ligand efficiency, and lipophilic efficiency of reference compound **2** (see Figure 1b, K_i = 200 nM, LE = 0.352, and LipE = 2.55). The second dashed line on scatter plot (a) shows the arbitrary threshold of 1 μM beyond which compounds are considered inactive.

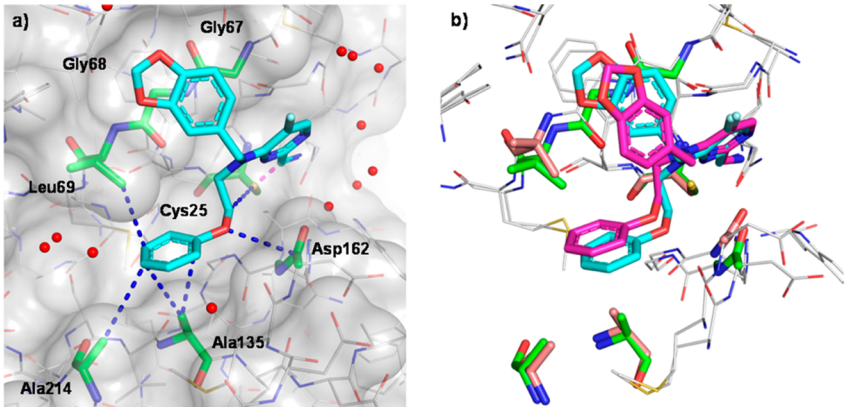

Figure 3. (a) Cocrystal structure of hCatL with compound **35** (PDB code 5MQY, resolution 1.13 Å). Short intermolecular contacts with distances of <4.0 Å between the ligand fragment (cyan) in the S2 pocket and protein residues (green) are shown as dashed blue lines. The covalent bond between the sulfur atom of Cys25 and the nitrile carbon atom of **35** is shown in magenta. Only water molecules with distances less than 5.0 Å from the ligand are shown. (b) Superimposition of the cocrystal structure of **35** in hCatL (ligand, cyan; protein, green) with a representative dominant pose from the FEP trajectory (ligand, magenta; protein, salmon).

and **37** are close neighbors of known hCatL inhibitors (Supporting Information Table S2) with Tanimoto similarities of 0.733, 0.729, and 0.717, respectively. The relative difficulty to identify this class is further put into context by the fact that it was prioritized by all four approaches. Molecules in class B are bigger and share a terminal aryl ring system which is connected to the main scaffold by a flexible propyl or oxyethyl linker (**30**, **31**, **33**–**35**, **38**). This class of compounds is also novel but was only prioritized by the FEP approach; **30**, **31**, **33**–**35**, **38** have Tanimoto similarities to known inhibitors of 0.614, 0.672, 0.629, 0.597, 0.672, and 0.642, respectively.

Analysis of the Cocrystal Structure of Fluoropyrimidine 35 in Complex with hCatL. The crystallographic binding mode of compound **35** in hCatL was determined to better understand the improved binding of these compounds (Figure 3a). As expected, the fluoropyrimidine nitrile warhead is engaged in a covalent bond with the sulfur atom of Cys25 and the piperonyl group sits in the S3 pocket engaging in π–π stacking interactions with the Gly67-Gly68 dipeptide at its base. The newly introduced ethoxybenzene substituent forms dispersive contacts with several hydrophobic side chains (Leu69, Ala135, Ala214) and the apolar surface of the backbone amide carbonyl of Asp162. In particular, the phenyl ring sits in a narrow cleft between residues Leu69 and Ala135. Several short contacts with distances from 3.4–3.7 Å suggest that this interaction region in the S2 pocket is important for the improved binding. It is also noteworthy that no obvious ligand strain is visible in the bound conformation. The C_{ar}–C_{ar}–O–C dihedral angle is close to planar (τ = 13°) and the O–C–C–N torsional angle adopts a gauche-like conformation (τ = 88°), which is in line with the preferred angle ranges derived from small molecule crystal structures.[22] Representative dominant

DOI: 10.1021/acs.jmedchem.6b01881
J. Med. Chem. XXXX, XXX, XXX–XXX

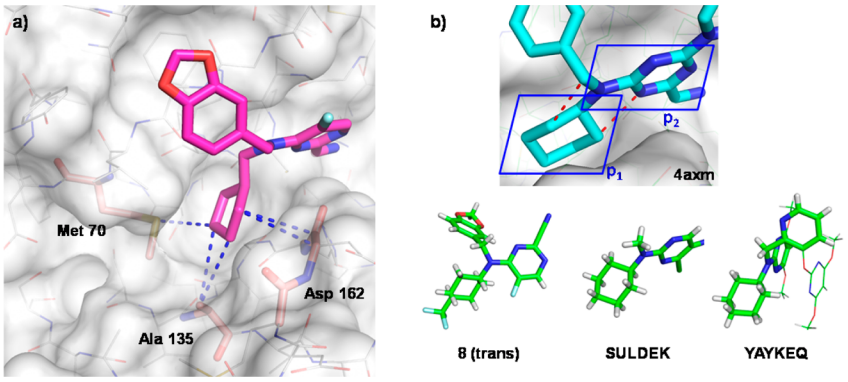

Figure 4. (a) Representative dominant pose from the FEP trajectory for compound **3** (ligand, magenta; protein, salmon). (b) Top: Cocrystal structure of hCatL with compound **1** (PDB code 4AXM). Short intramolecular contacts with distances of <2.8 Å in the ligand (cyan) are highlighted by red, dashed lines. The angle between the two planes p_1 and p_2 is 13°. Bottom: Small molecule crystal structures of representative molecules (green). The angles between p_1 and p_2 are 56° (**8**, trans), 89° (CSD code SULDEK), 56° (CSD code YAYKEQ), respectively.

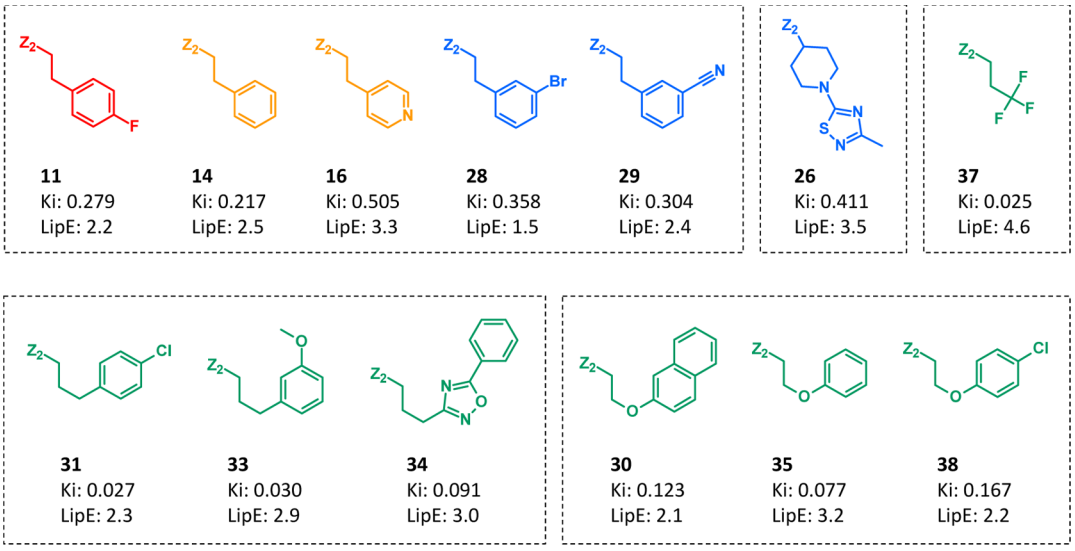

Figure 5. Novel substituents identified for the S2 pocket of hCatL. All fragments are shown for which the following two conditions for the full molecule are fulfilled: (a) K_i < 0.6 μM, (b) similarity to known fluoropyrimidine nitrile of <0.8. The fragments are colored by the selection method (MC = red, MM = orange, DOMF = blue, and FEP = green).

poses can be extracted from the molecular dynamics (MD) snapshots of the FEP trajectories. This was achieved by inspecting by eye 20 equally spaced frames of the molecular dynamics and selecting a consensus frame capturing the most common features. Figure 3b reveals a good agreement between the dominant FEP pose for compound **35** and its experimental binding mode (the pose was selected prior to the availability of the crystallographic data). While the protein−ligand interactions in the S2 pocket are very well reproduced, the main difference occurs in the orientation of the piperonyl ring system in the S3 pocket. The second, flipped orientation is also part of the FEP trajectory but to a smaller extent.

Ligand Conformations and Interactions of Most Active Molecules. Overall, the largest gain in binding affinity was achieved by a cyclopentylmethyl substituent in the S2 pocket (**3** K_i = 12 nM), which is 17-fold more active than the reference **2** (K_i = 200 nM). A representative dominant pose of the FEP trajectory of **3** is shown in Figure 4a. In contrast to the more extended topologies of class B compounds, the cyclopentyl group does not reach into the cleft between Leu69 and Ala135 but seems to optimally fill the front part of the S2 pocket. Five short dispersive interactions can be detected between the cyclopentyl group and protein atoms in this region (Met70, Ala135, backbone of Asp162). Apart from these favorable interactions, we suspect that some ligand strain in the bound conformation of reference **2** contributes to the large activity increase of compound **3**. This hypothesis is motivated by two very short intramolecular distances (d < 2.8 Å) observed in the hCatL cocrystal structure of **1** between atoms of the cyclohexyl ring and the scaffold (Figure 4b). The angle between the planes formed by the cyclohexyl substituent (p_1) and the aminotriazine scaffold (p_2) is close to planar (α = 13°), which is considerably smaller than those observed for similar topologies in the unbound conformation. For example, the small molecule crystal structure of compound **8** (trans) has α = 56° while other molecules in the CSD have even wider interplanar angles.

The three compounds (**3**, **22**, **37**) that improve LE relative to the reference all belong to class A occupying only the front part of the S2 pocket. This suggests that the selected class B molecules, which extend to the aromatic cleft and beyond into the back region of the S2 pocket, do not pick up as many favorable interactions as the best class A molecules and/or suffer from enthalpic or entropic penalties. The most active

DOI: 10.1021/acs.jmedchem.6b01881
J. Med. Chem. XXXX, XXX, XXX−XXX

class B molecules feature a relatively flexible propyl or ethoxy linker, which only partly occupies the front part of the S2 pocket. We suggest that in a next design step, the linker flexibility should be reduced, ideally in combination with improved protein interactions in the linker region. If successful, this would very likely increase the LE of class B molecules above the value of the reference molecule.

Novel hCatL Inhibitor Topologies and Hydrophobic Collapse. From our library selection exercise, several new molecular topologies to fill the S2 pocket of hCatL emerged (Figure 5). While aryl ring systems connected to the scaffold by a propyl or ethoxy linker are generally more potent compared to the ethyl linker analogues, the latter still show decent submicromolar hCatL activity and could provide an alternative starting point for medicinal chemistry optimization. Another interesting motif with a relatively high LipE of 3.5 for the full molecule is a thiadiazole attached to a piperidyl substituent.

After the release of the K_i values for the newly synthesized molecules, we revisited the results from the DOMF procedure which consisted of docking with subsequent postprocessing including minimization, rescoring, and filtering steps (see details in the Experimental Section). Since docking scores are notoriously uncorrelated with experimental binding affinities,[23−25] it is common practice to consider a rather large number of top-ranked docking solutions and to prune down to the final selection based on visual inspection of the suggested binding modes. Interestingly, we found that compound **33**, which is very potent in the enzymatic assay (K_i = 30 nM), was ranked at position 1 after postprocessing of the GOLD docking solution with Moloc[17] as well as after postprocessing with the Scorpion scoring function.[18] Although the potential favorable interactions of the terminal phenyl ring in the aromatic cleft of the S2 pocket were recognized in the docking pose, the compound was not selected because of potential hydrophobic collapse. This was triggered by earlier data mining studies in the CSD, which showed that phenyl rings connected by an unsubstituted propyl linker assume a collapsed conformation in 27% of all crystal structures with this motif (see details in the Methods Section). As the ligand needs to bind to hCatL in an extended conformation, clearly some energy penalty is involved in disrupting the collapsed conformation.

We then probed whether the FEP simulations of the unbound ligands in water show any signs of hydrophobic collapse (see details in the Methods Section). Taking the same geometric definition for collapse as in the CSD search, we found that for compounds **31** and **33**, which both have propyl linkers, the ratio of FEP snapshots with collapse to the total number of FEP snapshots is 27% and 64%, respectively. For the inhibitor **35**, which has an oxyethyl linker, the ratio from the FEP trajectory analysis is 14% while the CSD statistics for two phenyl rings connected by an unsubstituted oxyethyl linker is 9%. While the comparison between CSD statistics and FEP simulations is not trivial (they are carried out at very different temperatures and experimental conditions), it is encouraging to see that the FEP results are in the right ballpark and that the simulations are able to reproduce the higher propensity of unsubstituted propyl linkers to engage in hydrophobic collapse compared to the analogous oxyethyl linkers. The combined CSD and FEP analyses consistently suggest that an energy penalty has to be paid to break the collapsed conformations occurring in the unbound state but that this is more than compensated by favorable interactions with the protein, mainly in the aromatic cleft of the S2 pocket. Rigidification of the linker, for example, by replacement of sp^3 by sp^2 atoms or introduction of a substituent, can indeed reduce the propensity for hydrophobic collapse and its associated energy penalty. However, this depends strongly on the topology of the linker and further analyses on the specific linker system, as described here, would be needed to estimate the actual effect.

CONCLUSION

The purpose of our study was to evaluate the ability of FEP and other methods to prioritize potential hCatL reversible covalent inhibitors. This experiment was run in a fully prospective manner with synthesis and K_i determination of novel compounds and with time constraints relevant for therapeutic projects. Arguably the most important aspect of our FEP evaluation is the direct comparison with benchmark methods. In our case, we chose other computational selection methods well established in the industry as well as the selection of a medicinal chemist as references. We believe that similar types of benchmark comparisons are required to objectively assess the prediction power of FEP and to learn about its deficiencies.

In our study, FEP successfully picked 8 out of 10 compounds that were more potent than the reference, outperforming the different baselines, a medicinal chemist, and two typical modeling approaches. Interestingly, FEP was also able to identify one additional novel topology for S2 pocket moieties by correctly anticipating the extent to which compounds would be subject to hydrophobic collapse. That this effect was correctly handled is a clear sign of the soundness and usefulness of this approach. It also resulted in the most compelling knowledge gain from this study for that target: Additional designs based on the propyl- and oxyether-linked aryls would be an obvious follow-up.

From these results, we conclude that FEP is an attractive approach to prioritize compounds for synthesis, though our observation is based on this one single system. It should also be noted that the S2 binding pocket of hCatL has a strong lipophilic character and that additional studies are required to further substantiate if the type of results obtained here is also observed for more polar active sites.

One key point is that FEP scoring for this system was validated with retrospective literature data for this target before it was used prospectively. Without retrospective validation about the relevance and quality of its predictions, the outcome of the prospective FEP scoring is much less certain. With good evidence of its suitability, FEP appears well positioned to add significant value to industrial drug discovery projects. We also hope that our study design will further stimulate other prospective evaluations of FEP in different binding site environments and for alternative drug discovery use cases.

METHODS SECTION

Selection by a Medicinal Chemist (MC). Compounds were selected primarily on the basis of the existing SAR (Supporting Information Table 2 and refs 14−16), which already showed low double digit nM potencies for R = cyclohexyl and phenyl. Thus, phenyl **6** and *p*-fluorophenyl **7** as well as the structurally related *p*-chlorobenzyl **10** and *p*-fluorophenethyl **11** motifs were highlighted for synthesis. In order to probe whether a five-membered heterocyclic motif such as an oxazole is an appropriate replacement for the phenyl group, the structurally more distinct cyclopropyloxazole **12** was included. In addition, cyclohexyl side chains containing small

DOI: 10.1021/acs.jmedchem.6b01881
J. Med. Chem. XXXX, XXX, XXX−XXX

para substituents such as isopropyl- and CF_3-derivatives (**4** and **8**) as well as the tetrahydrothiopyran **9** were selected. To probe whether less spacious groups compared to cyclohexyl are tolerated, the cyclopentylmethyl **3** and methylcylopropyl **5** were picked. It should be noted that physicochemical properties such as solubility and lipophilicity were not guiding influences in this first round of compound selection. The whole process took our in-house expert less than 4 h.

Selection Based on Manual Modeling (MM). The MM selection was performed using the program Moloc and the all-atom MAB force field.[17] For each optimization, the protein coordinates and the covalent thioimidate were kept fixed. Next, the new ligands with the various S2 substituents were energy-minimized. While not all compounds of the library comprising 3325 amines could be modeled manually, an initial preselection of the ligands was performed based on their chemical structure and on the knowledge of S2 pocket SARs of the previously reported triazine nitriles.[14,16] In addition, conformationally flexible linkers to the amino group were limited to ethane-1,2-diyl and substituents with longer chains were not considered. A first set of ligands, **3**, **13**, and **17**, were selected to fill the S2 pocket with mainly aliphatic groups. A second set, **14**−**16** and **20**, features aromatic S2 substituents to undergo C−H···π interactions with Leu69. The substitution of phenyl (in **14**) by pyridyl (in **15** and **16**) reduces the predicted log *P* (clogP) of the ligand from 4.19 down to 3.04. Compounds **17**−**19** feature substituents which penetrate deeper inside the S2 pocket, compared to the previously reported ligands,[14,16] in order to harvest additional interactions with the protein. Biaryl ether **20** (clogP = 4.54), with appropriate torsional angle,[22] reaches deepest into the S2 pocket enabling the pyridine ring to intercalate between the side chains of Leu69 and Ala214.

The MM selection took a total of approximately 2 days: 1 day to manually prioritize compounds from the list of available building blocks and 1 day to finalize the selection by modeling compounds in Moloc.

Selection Based on Docking Followed by Manual Filtering (DOMF). One approach relied on small molecule docking into the hCatL crystal structure with subsequent filtering of the top-ranked solutions. We used GOLD[26,27] with the ChemPLP scoring function to generate binding poses in the protein structure 4AXM. To ensure proper orientation of the fluoropyrimidine nitrile warhead around the reactive Cys25, we employed a scaffold constraint with a weight of 5000 for the constant substructure of Figure 1d with 3D coordinates generated from the very similar ligand of complex structure 4AXM.[16] The nitrile was modeled with sp hybridization, and the side chain atoms of Cys25 were removed to avoid large steric clashes. An additional hydrophobic pharmacophore constraint (sphere radius of 2.0 Å, score contribution of 10 per atom in region) was placed in the S2 pocket at the center of the cyclohexyl ring of compound **2** to make sure that this apolar pocket, which is important for hCatL binding, is adequately sampled. Additional postprocessing was done by minimizing the docked solutions with Mol3d using the MAB force field,[17] and subsequent energy estimation with the ScorpionScore[18] energy function. The 100 top-ranked molecules from each of the three energy evaluations (ChemPLP, MAB, ScorpionScore) were combined, and highly constrained ligands with at least one torsional angle clearly outside the dihedral angle distribution of CSD small molecule crystal structures (red flag in program TorsionAnalyzer[28,29]) were removed. The docking poses of the remaining compounds were manually inspected using Moloc,[17] and 10 molecules, which were thought to have multiple favorable interactions with the protein while assuming a strain-free binding conformation, were finally selected.

Computation times for the individual steps were ∼13 h for docking and ∼2.5 h for postprocessing using a single CPU on a multicore Linux workstation (Intel Xeon E5-2650, 2.2 GHz). Manual filtering of the solutions required approximately 0.5 days.

Selection Based on FEP Scoring of Covalent Inhibitors (FEP). *Theoretical Framing of FEP Scoring of Covalent Ligands.* Covalent ligands bind to the protein through a two-step process. In the first step, the ligand binds to the protein active site due to electrostatic and hydrophobic interactions, forming a noncovalently bound protein−ligand prereaction complex. During the second step, a chemical reaction occurs between the warhead of the ligand and a protein residue in the binding pocket resulting in the formation of a covalent bond. Two distinct free energies are relevant to covalent ligand binding. The first is the binding free energy to form the prereaction complex, which is defined as the free energy difference between the protein−ligand prereaction complex and the separately solvated ligand and protein, denoted by ΔG_{n1} in Figure 6. The second is the free energy for covalent bond formation, which is defined as the free energy difference between the covalently bonded protein−ligand complex and protein−ligand prereaction complex, denoted by ΔG_{c1} in Figure 6. The overall binding free energy, which is the free energy difference between the covalently bonded protein−ligand complex and the state when the protein and ligand are separated in solution, is equal to the summation of the above two free energies.

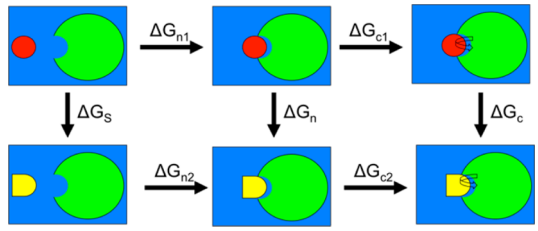

Figure 6. Thermodynamic cycle of covalent inhibitor binding.

In alchemical free energy calculations, the free energy difference between two states is calculated by gradually transforming the Hamiltonian from the first state to the second state. Through alchemical FEP simulations, we can calculate the free energy to mutate from ligand 1 to ligand 2 (in this context free energy refers to the Gibbs free energy) in bulk solution (ΔG_s in Figure 6), in the protein binding pocket (ΔG_n in Figure 6), as well as in the covalently bonded protein−ligand complexes (ΔG_c in Figure 6). Through the thermodynamic cycles shown in Figure 6, the relative binding free energy difference between two ligands for prereaction complex formation can be calculated by performing FEP simulations corresponding to the first two vertical legs of Figure 6, as is done is in the typical alchemical free energy calculations for noncovalent ligand binding. Similarly, by performance of FEP simulations corresponding to the first and the third vertical legs of Figure 6 (i.e., the difference of ΔG_s and ΔG_c), the relative overall binding free energy difference between the two reversible covalent ligands can also be directly obtained.

DOI: 10.1021/acs.jmedchem.6b01881
J. Med. Chem. XXXX, XXX, XXX−XXX

An example perturbation path for the calculation of the relative binding free energy between a pair of covalent ligands binding to hCatL is shown in Figure 7. In the first leg, the free

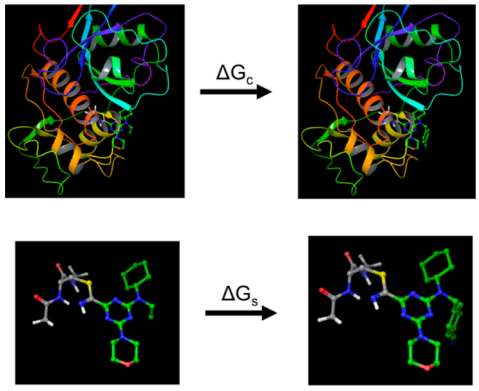

Figure 7. Example perturbation pathway for the calculation of relative binding free energy between a pair of covalent ligands binding to hCatL. Note, in the ΔG_s, that a fictitious dipeptide reference is used to ensure the interactions assigned to the dummy atoms are strictly identical in the complex and solvent legs of the FEP simulations.

energy to mutate from the covalently bonded protein−ligand 1 complex to protein−ligand 2 complex is calculated, and in the second leg, the free energy to mutate from ligand 1 to ligand 2 in bulk solution is calculated. The difference between the two free energies gives the relative binding free energy of the two ligands.

When comparing the relative overall binding free energy calculated in this way to experimental data, we are assuming that the concentration of the protein−ligand prereaction complex does not appreciably contribute to the experimentally measured affinity. In practice, the protein−ligand prereaction complex might also contribute to the measured affinity; however, if the equilibrium concentration of the protein−ligand prereaction complex is much smaller than that of the covalently bonded complex, the contribution should be negligible.

It should also be noted that the covalent bond between the warhead of the ligand and the corresponding protein residue is modeled by a harmonic potential in classical-mechanics-based force fields. Therefore, the free energy difference between the ligands due to the changing reactivity of the different warheads, which is mainly due to quantum effects, cannot be accurately modeled in this protocol. Thus, the above method should only be accurate for the calculation of relative binding free energies between covalent ligands with the same warhead and when the mutation is relatively far away from the warhead. This is the case in the study presented here.

Details of the FEP Simulation. The FEP+ product implemented in Schrodinger software suite was used for all the simulations.[7] The PDB structure 4AXM was prepared with the Protein Preparation Wizard program assuming a pH of 7 and used as the starting structure for all simulations. The OPLS3 force field was used for the protein and ligands, and the SPC water model was used for solvent.[8] The systems were relaxed by a series of short MD simulations through the standard relaxation protocol implemented in FEP+ reported in prior publications.[7,30] A total number of 12 λ windows were used for both the complex and solvent simulations, and the production simulations lasted 5 ns for each λ window. The FEP/REST method reported in a prior publications was used to enhance the sampling of protein−ligand binding pocket,[7,30] and the Bennett acceptance ratio method was used to calculate the free energy difference between neighboring λ windows.

Docking and Compound Selection for FEP Analysis. The PDB structure 4AXM was prepared with the Protein Preparation Wizard program assuming a pH of 7 and used as the starting structure for all docking analyses. The cocrystallized ligand was modified to coincide with its prereactive form, and the catalytic residue Cys25 was mutated to alanine to accommodate the additional steric bulk of the reactive nitrile. All 3325 ligand design ideas were docked in the active site of the modified 4AXM structure using Glide SP core constrained docking to the modified cocrystallized ligand.[31] Of these 3325 virtual ligands, 2258 did not return a valid docking pose, due to severe steric clashes and other distortions while respecting the core constraints. The 1067 compounds that were found to dock successfully were carried forward to MM-GB/SA scoring.[32] The *Z*-score data fusion method was used to combine the MM-GB/SA and Glide SP scores for these ligands into a single composite score.[32] A human expert was asked to select a diverse set of ∼100 molecules for FEP+ scoring. In consultation with the human expert, 93 molecules were ultimately scored, and the top scoring of these were recommended for synthesis. A table detailing the ranks of the synthesized molecules in the original 1067 Glide SP, MM-GB/SA, and *Z*-score rank-ordered lists may be found in Table 3.

Table 3. Ranks of the Molecules Selected for Synthesis on the Basis of the FEP+ Scoring in the Glide SP, MM-GB/SA, and *Z*-Score Rank Ordered Lists[a]

compd	Glide SP rank	MM-GB/SA rank	*Z*-score rank
3	189	501	267
37	99	691	265
35	62	303	96
33	17	37	8
31	31	177	35
30	8	488	55
36	28	284	56
34	44	133	38
32	412	94	187

[a]Molecule **38** differed from the originally submitted molecule by omission of a CH_2 linker carbon, and its rank in the triage process is thus unavailable.

Computation Time. The docking and MM-GB/SA steps, including the human time investment, took approximately 2 days using standard computing resources. Determining the binding free energies of the 93 selected molecules took 7360 GPU hours on K80 equivalent GPUs or approximately 5 days of exclusive access to a 64 GPU cluster. Human time required to ensure atom mappings and interaction mappings were correct for all FEP calculations reported herein was significant. However, the laborious parts of this step have been fully automated over the course of completing this work, and only minimal human time would be required to run similar covalent inhibitor R-group optimizations in the future.

Similarity Calculation. The similarity between two molecules was determined by calculating the Tanimoto value[33] between their ECFP4 descriptors.[34] The set of known hCatL fluoropyrimidine nitrile inhibitors was compiled by grouping the 13 different substituents previously reported (see

DOI: 10.1021/acs.jmedchem.6b01881
J. Med. Chem. XXXX, XXX, XXX−XXX

Scheme 1. Synthesis of Fluoropyrimidine Nitriles 3−38[a]

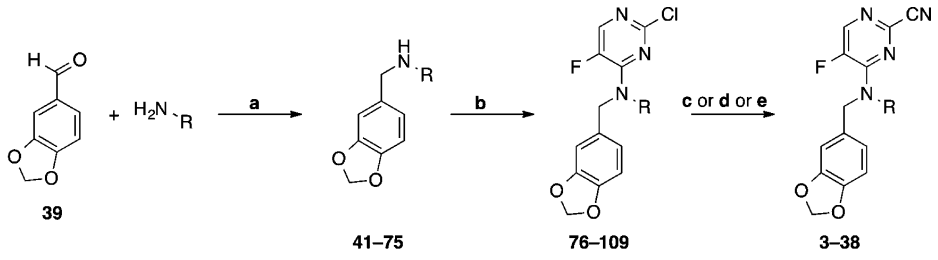

a: 1) mol. sieves 4 Å, (1 eq. TEA), CH_2Cl_2, 25 °C, 10 −16 h, 2) $NaBH(OAc)_3$ (2.5 eq.), CH_2Cl_2, 25 °C, 10–16 h;
b: 2,4-dichloro-5-fluoropyrimidine, iPr_2NEt (1.2 eq.), *i*PrOH/EtOH 2:1, 80 °C,10–16 h;
c: G3-*t*BuXPhos precatalyst (0.05 eq.), $Zn(CN)_2$ (0.66 eq.), THF/H_2O 1:5; 50 °C,6–18 h;
d: G3-*t*BuXPhos precatalyst (0.05 eq.), $Zn(CN)_2$ (0.66 eq.), DMF; 60 °C,12 h;
e: KCN (1 eq.), DABCO (1 eq.), DMSO/H_2O 9:1, 60 °C, 55 h.

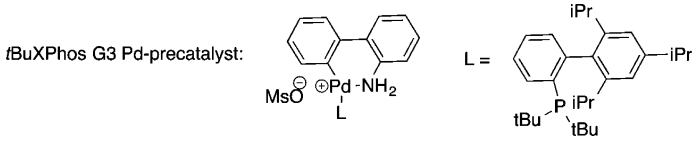

[a]DMSO = dimethylsulfoxide, DMF = *N*,*N*-dimethylformamide, DABCO = 1,4-diazabicyclo[2.2.2]octane, TEA = triethylamine.

Supporting Information Table S2) and replacing their core by the fluoropyrimidine nitrile used in this study. The resulting set of 13 compounds is virtual but correctly defines the known chemical space (this is why compound **6** has a Tanimoto similarity of 1.0 in Table 2). The similarity between each molecule prioritized and the closest known fluoropyrimidine nitrile was calculated by determining the similarity between that molecule and all eight reference molecules and keeping the maximum value. The similarity between sets of molecules (complete list and MC, MM, DOMF, and FEP selections) was computed by calculating the maximum similarity between each molecule in the set, in turn, and the eight reference compounds and determining the arithmetic mean of those Tanimoto scores.

Investigation of Hydrophobic Collapse. Experimental propensities to form conformations of hydrophobic collapse were derived by data mining of the CSD, version 5.33, using the ConQuest 1.14 program. The following general search flags were set: $R \leq 0.10$, "3D coordinates determined", "not disordered", "no ions", "no errors", "not polymeric", and "only organic". The two molecular topologies investigated for this study were two phenyl rings A and B connected by an unsubstituted *n*-propyl and oxyethyl linker, respectively. The propensity for a given topology to form hydrophobic collapse was calculated from the ratio of CSD entries showing a collapsed conformation to the total number of entries. A CSD crystal structure conformation was considered collapsed if at least three distances *d* between any atom of phenyl ring A and any atom of phenyl ring B fulfilled $d \leq 4.0$ Å. We verified this definition in model systems of parallel-displaced and edge-to-face arrangements, and this seemed to be more general compared to definitions using ring centroids.

FEP simulations of the solvent leg were analyzed for hydrophobic collapse using the same geometric criteria as in the CSD searches. A total of 22 snapshots were taken into account for each ligand investigated. These snapshots were taken from 20 equally spaced frames of the 5 ns solvent leg production stage FEP simulation and included data from λ_0 and λ_{11} windows where a single ligand species is simulated in each window.

EXPERIMENTAL SECTION

Synthesis of the Fluoropyrimidine Derivatives. The series of 37 5-fluoropyrimidinenitriles **3**−**38** (except **12**) was prepared by a three-step protocol based on reductive amination, nucleophilic aromatic substitution, and palladium-catalyzed cyanation (see Scheme 1). The first two steps relied on procedures previously reported for the synthesis of triazine nitriles.[16] Reductive amination of piperonal and corresponding primary amines gave all the desired secondary amines **41**−**75** in good to excellent yields (Supporting Information Tables S4−S6). Nucleophilic substitution of 2,4-dichloro-5-fluoropyrimidine with secondary amines in the presence of Hünig base in *i*-PrOH/EtOH 2:1 furnished 2-chloropyrimidin-4-amines **76**−**109** with yields in broad range 23−97% (Supporting Information Table S5).

Final nitriles were synthesized by palladium-catalyzed cyanation using Buchwald third generation Pd-precatalyst *t*-BuXPhos and $Zn(CN)_2$ as a cyanide source in a mixture of THF and water 1:5 at 50 °C.[35] In the case of ligands containing a second chlorine atom in the molecule (**10**, **31**, **36**, **38**), only 0.5 equiv of $Zn(CN)_2$ was used to avoid dicyanation. DMF was employed as a solvent for the synthesis of ligands **4** and, **9**, which are insoluble in the THF/water mixture.

Palladium-catalyzed cyanation failed in the cases of ligands **28** and, **34**. These two ligands were instead prepared by nucleophilic substitution with KCN in the presence of DABCO in a DMSO/water mixture. Reactions had to be performed at lower temperature (60 °C) to avoid decomposition and for longer reaction times (3 days) than in the published procedure[15] to get ligands **28** and, **34** in low yields (14% and 43%, respectively). Detailed synthesis, yields, cyanation optimization, and characterization of all compounds are available in the Supporting Information.

Chemical Synthesis. All reagents were purchased from commercial suppliers and used without further purification. Primary amines for the synthesis were provided by F. Hoffmann-La Roche Ltd. and were used as received. Solvents for the synthesis were purchased in HPLC quality, and solvents for extractions and chromatography were of technical grade and were distilled prior to use. Thin layer chromatography (TLC) was conducted on aluminum sheets coated with SiO_2 60 F_{254} (Merck), visualization with UV lamp (254 nm) or by ninhydrin staining (1.5 g in 100 mL of *n*-butanol and 3 mL of glacial acetic acid). MPLC was performed on an ISCO Combiflash Rf 200 system on RediSep Rf normal-phase silica flash columns (particle size 35−70 μm, 230−400 mesh). HPLC analysis was performed on a Merck Hitachi LaChrom HPLC system (D-7000 interface, L-7100 pump, L-7200 autosampler, and L-7400 UV detector). Separations under acidic conditions (HPLC method A) were performed using

DOI: 10.1021/acs.jmedchem.6b01881
J. Med. Chem. XXXX, XXX, XXX−XXX

0.1% vol formic acid in eluent H_2O and MeCN on a Merck Superspher 100 RP-18e (100 Å, 4 μm), 250 mm × 4 mm column. Separations under basic conditions (HPLC method B) were performed using a 10 mM K_2HPO_4 buffer (pH 8) in eluent H_2O and MeCN/H_2O (7:3) on a SGE ProteCol C18H (120 Å, 5 μm) 250 mm × 4.6 mm column. A flow rate of 1 mL/min was used, and the UV detector was set to 254 nm (optical path length of 10 mm). Melting points (mp) were measured on a Büchi M-560 melting point apparatus in open capillaries and are uncorrected. Infrared spectra (IR) were recorded on a PerkinElmer Spectrum Two FT-IR device fitted with an ATR unit (4000−600 cm^{-1}). Absorption bands are given in wavenumbers (cm^{-1}), and signal intensities are specified with s (strong), m (medium), and w (weak). NMR spectra were measured on a Varian Gemini 300 MHz spectrometer (300 MHz for ^1H and 75 MHz for ^{13}C) or a Bruker DRX 400 MHz spectrometer (400 MHz for ^1H, 100 MHz for ^{13}C, and 376 MHz for ^{19}F) in $CDCl_3$ (referenced to the residual solvent signal, $CDCl_3$, δ H = 7.26, δ C = 77.16 ppm) at 25 °C. Chemical shifts are given in ppm (δ scale), coupling constants (J) in Hz. Complete assignment of all NMR signals was performed using a combination of H,H-COSY, H,C-HSQC, and H,C-HMBC experiments. High-resolution electrospray ionization mass spectrometry (HR-ESI-MS) was conducted with a Bruker Daltonics maXis ESI/Nanospray Qq TOF instrument. All mass spectra were acquired by the MS service of the Laboratory of Organic Chemistry at ETH Zurich. Elemental analyses were performed by the Mikrolabor of the Laboratory of Organic Chemistry at ETH Zurich with a LECO CHNS/932 instrument. Purity of all final compounds (>95%) was determined by elemental analyses or by analytical HPLC. The nomenclature was obtained with ACD/Name software (ACD/Labs).

General Procedure A: Reductive Amination. A solution of the primary amine (1.0 equiv) and piperonal (**39**) (0.9 equiv) in CH_2Cl_2 (3.5 mL/1 mmol of amine) over molecular sieves (4 Å) (if starting material was a hydrochloride salt, triethylamine (1.0 equiv) was added) was stirred at 25 °C for 10−18 h, treated with $NaBH(OAc)_3$ (2.5 equiv), and stirred at 25 °C for another 10−18 h. The mixture was diluted with CH_2Cl_2 and sat. $NaHCO_3$ solution and filtered. The organic layer was washed with sat. $NaHCO_3$ solution (3×), dried over Na_2SO_4, filtered, and evaporated. The crude material was purified by MPLC.

General Procedure B: Nucleophilic Aromatic Substitution. The secondary amine (1.0 equiv) and 2,4-dichloro-5-fluoropyrimidine (**40**) (1.0 equiv) were dissolved in *i*-PrOH or *i*-PrOH/EtOH (2:1) (5.0 mL/1 mmol of amine), *i*-Pr_2NEt (1.2 equiv) was added, and the mixture was heated at 85 °C for 18−24 h. Solvents were evaporated, and the crude material was purified by MPLC.

General Procedure C: Palladium-Catalyzed Cyanation in THF/H_2O.[35] A Biotage microvawe reaction vial (2−5 mL) was charged with a 2-chloro-5-fluoro-4-pyrimidinamine (1.0 equiv), $Zn(CN)_2$ (0.66 equiv or 0.5 equiv if the pyrimidinamine contained an additional chlorine atom), and *t*-BuXPhos G3 Pd-precatalyst (0.05 equiv). The vial was capped with septum, evacuated, and refilled with argon. THF/degassed H_2O 1:5 (3 mL/0.2 mmol of pyrimidinamine) was added, and the mixture was vigorously stirred (1200 rpm) at 60 °C for 12−18 h. Efficient stirring is crucial for complete conversion. The mixture was diluted with sat. $NaHCO_3$ solution (2 mL) and EtOAc (2 mL) and stirred for 5 min. The layers were separated, and the aqueous layer was extracted with EtOAc (3 × 2 mL). The combined organic layers were dried over Na_2SO_4, filtered, and evaporated. The crude material was purified by MPLC.

General Procedure D: Palladium-Catalyzed Cyanation in DMF. A Biotage microwave reaction vial (2−5 mL) was charged with a 2-chloro-5-fluoro-4-pyrimidinamine (1.0 equiv), $Zn(CN)_2$ (0.66 equiv), and *t*-BuXPhos G3 Pd-precatalyst (0.05 equiv). The vial was capped with septum, evacuated, and refilled with argon. DMF (4 mL/0.5 mmol of pyrimidinamine) was added, and the mixture was stirred at 60 °C for 1−12 h. The solvent was coevaporated with toluene, and the crude product was purified by MPLC.

Determination of hCatL Activity. The inhibitory constants (K_i) of the ligands against hCatL were calculated using the Cheng−Prusoff equation[36] from the IC_{50} determined in an enzymatic assay following the same procedure as previously described.[15]

Cocrystallization of hCatL in Complex with Ligand 35 (PDB code 5MQY). Protein at a concentration of 6.7 μM in 100 mM sodium acetate, pH 5.5, 5 mM DTT, 5 mM EDTA, 0.02% NaN_3 (buffer A) was incubated with **35** in a 12-fold molar excess overnight at 4 °C under argon. Subsequently the protein−ligand solution was diluted by addition of 100 mL of buffer A and further incubated for 2 h at 21 °C. Precipitated material was removed by centrifugation. Prior to crystallization experiments, the protein−ligand mixture was concentrated to 30.4 mg/mL and centrifuged at 20 000*g*. The crystallization droplets were set up at 21 °C by mixing 0.1 μL of protein solution with 0.17 μL of reservoir solution and 0.03 μL of seed solution of CatL crystals in sitting drop vapor diffusion experiments. Crystals were obtained within 1 day out of 25% PEG 3350, 0.1 M Bis-Tris, pH 6.5.

■ ASSOCIATED CONTENT

Supporting Information

. The Supporting Information is available free of charge on the ACS Publications website at DOI: 10.1021/acs.jmedchem.6b01881.

Molecular strings and some data (CSV)

List of all virtual molecules to prioritize, previsously known SAR for the hCatL triazine series, retrospective validation of FEP+ approach, chemical diagrams of CSD structures SULDEK and YAYKEQ, compound characterization, yields, cyanation optimization, small molecule X-ray crystallography (PDF)

Accession Codes

Atomic coordinates and experimental data for the cocrystal structure of **35** (PDB code 5MQY) in complex with hCatL will be released upon article publication.

■ AUTHOR INFORMATION

Corresponding Authors

*R.A.: phone, +1 212 548 2352; e-mail, robert.abel@schrodinger.com.

*F.D.: phone, +41 44 63 22992; e-mail, diederich@org.chem.ethz.ch.

*J.H.: phone, +41 61 68 89773; e-mail, jerome.hert@roche.com.

ORCID

Michal Tichý: 0000-0002-8460-7680

Lingle Wang: 0000-0002-8170-6798

Rainer E. Martin: 0000-0001-7895-497X

Jérôme Hert: 0000-0003-3062-8029

Author Contributions

#B.K., M.T., and L.W. contributed equally. The manuscript was written through contributions of all authors. All authors have given approval to the final version of the manuscript.

Notes

The authors declare no competing financial interest.

■ ACKNOWLEDGMENTS

We thank Dr. Bruno Bernet for help with the compound characterizations, Dr. Nils Trapp for small molecule crystallography, and Dr. Julian Fuchs for help in deriving CSD statistics for the investigation of hydrophobic collapse. Work at ETH Zurich was supported by a grant from the ETH Research Council (Grant ETH-01 13-2) and by an F. Hoffmann-La Roche−ETH Zurich research agreement.

DOI: 10.1021/acs.jmedchem.6b01881
J. Med. Chem. XXXX, XXX, XXX−XXX

ABBREVIATIONS USED

CSD, Cambridge Structural Database; DOMF, docking and manual filtering; ECFP, extended-connectivity fingerprints; FEP, free energy perturbation; hCatL, human cathepsin L; HR-ESI-MS, high-resolution electrospray ionization mass spectrometry; LipE, lipophilic efficiency; MC, medicinal chemist; MM, manual modeling; MM-GB/SA, molecular mechanics generalized Born/surface area; MPLC, medium pressure liquid chromatography

REFERENCES

(1) Postma, J. P. M.; Berendsen, H. J. C.; Haak, J. R. Thermodynamics of Cavity Formation in Water. A Molecular Dynamics Study. *Faraday Symp. Chem. Soc.* **1982**, *17*, 55−67.

(2) Tembre, B. L.; Mc Cammon, J. A. Ligand-Receptor Interactions. *Comput. Chem.* **1984**, *8*, 281−283.

(3) Jorgensen, W. L.; Ravimohan, C. Monte Carlo Simulation of Differences in Free Energies of Hydration. *J. Chem. Phys.* **1985**, *83*, 3050−3054.

(4) Kollman, P. Free Energy Calculations: Applications to Chemical and Biochemical Phenomena. *Chem. Rev.* **1993**, *93*, 2395−2417.

(5) Kollman, P. A.; Massova, I.; Reyes, C.; Kuhn, B.; Huo, S.; Chong, L.; Lee, M.; Lee, T.; Duan, Y.; Wang, W.; Donini, O.; Cieplak, P.; Srinivasan, J.; Case, D. A.; Cheatham, T. E. III. Calculating Structures and Free Energies of Complex Molecules: Combining Molecular Mechanics and Continuum Models. *Acc. Chem. Res.* **2000**, *33*, 889−897.

(6) Gallicchio, E.; Levy, R. M. Advances in All Atom Sampling Methods for Modeling Protein−Ligand Binding Affinities. *Curr. Opin. Struct. Biol.* **2011**, *21*, 161−166.

(7) Wang, L.; Wu, Y.; Deng, Y.; Kim, B.; Pierce, L.; Krilov, G.; Lupyan, D.; Robinson, S.; Dahlgren, M. K.; Greenwood, J.; Romero, D. L.; Masse, C.; Knight, J. L.; Steinbrecher, T.; Beuming, T.; Damm, W.; Harder, E.; Sherman, W.; Brewer, M.; Wester, R.; Murcko, M.; Frye, L.; Farid, R.; Lin, T.; Mobley, D. L.; Jorgensen, W. L.; Berne, B. J.; Friesner, R. A.; Abel, R. Accurate and Reliable Prediction of Relative Ligand Binding Potency in Prospective Drug Discovery by Way of a Modern Free-Energy Calculation Protocol and Force Field. *J. Am. Chem. Soc.* **2015**, *137*, 2695−2703.

(8) Harder, E.; Damm, W.; Maple, J.; Wu, C.; Reboul, M.; Xiang, J. Y.; Wang, L.; Lupyan, D.; Dahlgren, M. K.; Knight, J. L.; Kaus, J. W.; Cerutti, D. S.; Krilov, G.; Jorgensen, W. L.; Abel, R.; Friesner, R. A. PLS3: A Force Field Providing Broad Coverage of Drug-like Small Molecules and Proteins. *J. Chem. Theory Comput.* **2016**, *12*, 281−296.

(9) Homeyer, N.; Stoll, F.; Hillisch, A.; Gohlke, H. Binding Free Energy Calculations for Lead Optimization: Assessment of Their Accuracy in an Industrial Drug Design Context. *J. Chem. Theory Comput.* **2014**, *10*, 3331−3344.

(10) Steinbrecher, T. B.; Dahlgren, M.; Cappel, D.; Lin, T.; Wang, L.; Krilov, G.; Abel, R.; Friesner, R.; Sherman, W. Accurate Binding Free Energy Predictions in Fragment Optimization. *J. Chem. Inf. Model.* **2015**, *55*, 2411−2420.

(11) Ciordia, M.; Pérez-Benito, L.; Delgado, F.; Trabanco, A. A.; Tresadern, G. Application of Free Energy Perturbation for the Design of BACE1 Inhibitors. *J. Chem. Inf. Model.* **2016**, *56*, 1856−1871.

(12) Lovering, F.; Aevazelis, C.; Chang, J.; Dehnhardt, C.; Fitz, L.; Han, S.; Janz, K.; Lee, J.; Kaila, N.; McDonald, J.; Moore, W.; Moretto, A.; Papaioannou, N.; Richard, D.; Ryan, M. S.; Wan, Z.-K.; Thorarensen, A. Imidazotriazines: Spleen Tyrosine Kinase (Syk) Inhibitors Identified by Free-Energy Perturbation (FEP). *ChemMedChem* **2016**, *11*, 217−233.

(13) Abel, R.; Mondal, S.; Masse, C.; Greenwood, J.; Harriman, G.; Ashwell, M. A.; Bhat, S.; Wester, R.; Frye, L.; Kapeller, R.; Friesner, R. A. Accelerating Drug Discovery through Tight Integration of Expert Molecular Design and Predictive Scoring. *Curr. Opin. Struct. Biol.* **2017**, *43*, 38−44.

(14) Ehmke, V.; Heindl, C.; Rottmann, M.; Freymond, C.; Schweizer, W. B.; Brun, R.; Stich, A.; Schirmeister, T.; Diederich, F. Potent and Selective Inhibition of Cysteine Proteases from *Plasmodium Falciparum* and *Trypanosoma Brucei*. *ChemMedChem* **2011**, *6*, 273−278.

(15) Ehmke, V.; Quinsaat, J. E. Q.; Rivera-Fuentes, P.; Heindl, C.; Freymond, C.; Rottmann, M.; Brun, R.; Schirmeister, T.; Diederich, F. Tuning and Predicting Biological Affinity: Aryl Nitriles as Cysteine Protease Inhibitors. *Org. Biomol. Chem.* **2012**, *10*, 5764−5768.

(16) Ehmke, V.; Winkler, E.; Banner, D. W.; Haap, W.; Schweizer, W. B.; Rottmann, M.; Kaiser, M.; Freymond, C.; Schirmeister, T.; Diederich, F. Optimization of Triazine Nitriles as Rhodesain Inhibitors: Structure-Activity Relationships, Bioisosteric Imidazopyridine Nitriles, and X-Ray Crystal Structure Analysis with Human Cathepsin L. *ChemMedChem* **2013**, *8*, 967−975.

(17) Gerber, P. R.; Müller, K. MAB, a Generally Applicable Molecular Force Field for Structure Modelling in Medicinal Chemistry. *J. Comput.-Aided Mol. Des.* **1995**, *9*, 251−268.

(18) Kuhn, B.; Fuchs, J. E.; Reutlinger, M.; Stahl, M.; Taylor, N. R. Rationalizing Tight Ligand Binding through Cooperative Interaction Networks. *J. Chem. Inf. Model.* **2011**, *51*, 3180−3198.

(19) Vicik, R.; Busemann, M.; Baumann, K.; Schirmeister, T. Inhibitors of Cysteine Proteases. *Curr. Top. Med. Chem.* **2006**, *6*, 331−353.

(20) Hopkins, A. L.; Groom, C. R.; Alex, A. Ligand Efficiency: A Useful Metric for Lead Selection. *Drug Discovery Today* **2004**, *9*, 430−431.

(21) Leeson, P. D.; Springthorpe, B. The Influence of Drug-like Concepts on Decision-Making in Medicinal Chemistry. *Nat. Rev. Drug Discovery* **2007**, *6*, 881−890.

(22) Brameld, K. A.; Kuhn, B.; Reuter, D. C.; Stahl, M. Small Molecule Conformational Preferences Derived from Crystal Structure Data. A Medicinal Chemistry Focused Analysis. *J. Chem. Inf. Model.* **2008**, *48*, 1−24.

(23) Perola, E.; Walters, W. P.; Charifson, P. S. A Detailed Comparison of Current Docking and Scoring Methods on Systems of Pharmaceutical Relevance. *Proteins: Struct., Funct., Genet.* **2004**, *56*, 235−249.

(24) Plewczynski, D.; Łaźniewski, M.; Augustyniak, R.; Ginalski, K. Can We Trust Docking Results? Evaluation of Seven Commonly Used Programs on PDBbind Database. *J. Comput. Chem.* **2011**, *32*, 742−755.

(25) Gathiaka, S.; Liu, S.; Chiu, M.; Yang, H.; Stuckey, J. A.; Kang, Y. N.; Delproposto, J.; Kubish, G.; Dunbar, J. B., Jr; Carlson, H. A.; Burley, S. K.; Walters, W. P.; Amaro, R. E.; Feher, V. A.; Gilson, M. K. D3R Grand Challenge 2015: Evaluation of Protein−Ligand Pose and Affinity Predictions. *J. Comput.-Aided Mol. Des.* **2016**, *30*, 651−668.

(26) Jones, G.; Willett, P.; Glen, R. C. Molecular Recognition of Receptor Sites Using a Genetic Algorithm with a Description of Desolvation. *J. Mol. Biol.* **1995**, *245*, 43−53.

(27) Jones, G.; Willett, P.; Glen, R. C.; Leach, A. R.; Taylor, R. Development and Validation of a Genetic Algorithm for Flexible Docking. *J. Mol. Biol.* **1997**, *267*, 727−748.

(28) Schärfer, C.; Schulz-Gasch, T.; Ehrlich, H.-C.; Guba, W.; Rarey, M.; Stahl, M. Torsion Angle Preferences in Druglike Chemical Space: A Comprehensive Guide. *J. Med. Chem.* **2013**, *56*, 2016−2028.

(29) Guba, W.; Meyder, A.; Rarey, M.; Hert, J. Torsion Library Reloaded: A New Version of Expert-Derived SMARTS Rules for Assessing Conformations of Small Molecules. *J. Chem. Inf. Model.* **2016**, *56*, 1−5.

(30) Wang, L.; Deng, Y.; Knight, J. L.; Wu, Y.; Kim, B.; Sherman, W.; Shelley, J. C.; Lin, T.; Abel, R. Modeling Local Structural Rearrangements Using FEP/REST: Application to Relative Binding Affinity Predictions of CDK2 Inhibitors. *J. Chem. Theory Comput.* **2013**, *9*, 1282−1293.

(31) Friesner, R. A.; Banks, J. L.; Murphy, R. B.; Halgren, T. A.; Klicic, J. J.; Mainz, D. T.; Repasky, M. P.; Knoll, E. H.; Shelley, M.; Perry, J. K.; Shaw, D. E.; Francis, P.; Shenkin, P. S. Glide: A New

DOI: 10.1021/acs.jmedchem.6b01881
J. Med. Chem. XXXX, XXX, XXX−XXX

Approach for Rapid, Accurate Docking and Scoring. 1. Method and Assessment of Docking Accuracy. *J. Med. Chem.* **2004**, *47*, 1739−1749.
(32) Knight, J. L.; Krilov, G.; Borrelli, K. W.; Williams, J.; Gunn, J. R.; Clowes, A.; Cheng, L.; Friesner, R. A.; Abel, R. Leveraging Data Fusion Strategies in Multireceptor Lead Optimization MM/GBSA End-Point Methods. *J. Chem. Theory Comput.* **2014**, *10*, 3207−3220.
(33) Willett, P.; Barnard, J. M.; Downs, G. M. Chemical Similarity Searching. *J. Chem. Inf. Comput. Sci.* **1998**, *38*, 983−996.
(34) Rogers, D.; Hahn, M. Extended-Connectivity Fingerprints. *J. Chem. Inf. Model.* **2010**, *50*, 742−754.
(35) Cohen, D. T.; Buchwald, S. L. Mild Palladium-Catalyzed Cyanation of (Hetero)aryl Halides and Triflates in Aqueous Media. *Org. Lett.* **2015**, *17*, 202−205.
(36) Cheng, Y.-C.; Prusoff, W. H. Relationship between the Inhibition Constant (KI) and the Concentration of Inhibitor Which Causes 50 per Cent Inhibition (I50) of an Enzymatic Reaction. *Biochem. Pharmacol.* **1973**, *22*, 3099−3108.

DOI: 10.1021/acs.jmedchem.6b01881
J. Med. Chem. XXXX, XXX, XXX−XXX